Journal of Power Sources 222 (2013) 59–65

Contents lists available at SciVerse ScienceDirect

Journal of Power Sources

journal homepage: www.elsevier.com/locate/jpowsour

Lysine-assisted hydrothermal synthesis of hierarchically porous Fe_2O_3 microspheres as anode materials for lithium-ion batteries

Jingjing Zhang, Yifan Sun, Yu Yao, Tao Huang*, Aishui Yu*

Department of Chemistry, Shanghai Key Laboratory of Molecular Catalysis and Innovative Materials, Institute of New Energy, Fudan University, Shanghai 200438, China

HIGHLIGHTS

- Fe_2O_3 microspheres were prepared by a simple, template-free hydrothermal method.
- Hierarchical porous Fe_2O_3 microspheres are assembled by uniform nanoparticles.
- Lysine acts as a hydrolysis-controlling agent.
- The Fe_2O_3 microspheres have a high capacity of 705 mA h g^{-1} at 430th cycle.

ARTICLE INFO

Article history:
Received 11 May 2012
Received in revised form
17 August 2012
Accepted 21 August 2012
Available online 28 August 2012

Keywords:
Lithium-ion battery
Anode material
Hematite
Microsphere
Lysine

ABSTRACT

A novel lysine-assisted hydrothermal process is first developed to produce hierarchically porous Fe_2O_3 microspheres assembled by well-crystalline nanoparticles. The fabrication process is very simple, without employing any surfactants or templates. A possible growth mechanism of the nano/microspherical superstructure is further discussed. The contribution of lysine to the formation of the unique microspheres is also tentatively proposed. Furthermore, as an anode electrode material for rechargeable lithium-ion batteries, the Fe_2O_3 microsphere displays excellent electrochemical performance. It also exhibits the feature of capacity increase upon cycling and shows a stable and reversible capacity of 705 mA h g^{-1} after 430 cycles. The outstanding electrochemical performance of the Fe_2O_3 microsphere can be attributed to the hierarchical porosity, ordered microstructure, good electron pathways and easy penetration of the electrolyte.

1. Introduction

Lithium-ion batteries (LIBs), with high energy and power densities, are in great demand as energy sources for many applications such as hybrid vehicles and clean energy storage [1–4]. Transition-metal oxides (MO, where M is Fe, Co, Ni, Cu, etc.) have emerged as potential anode materials for LIBs because they deliver a theoretical specific capacity far larger than that of commercial graphite material (372 mA h g^{-1}). It has been considered that such a large capacity can be attributed to the conversion reaction [5,6], which is different from the intercalation mechanism in traditional LIBs system. Among these metal oxides, Fe_2O_3 has attracted considerable attention due to its low cost, huge abundance on earth, environmental benignity and high theoretical specific capacity (1007 mA h g^{-1}) [7–12]. Unfortunately, the practical application of Fe_2O_3 in LIBs is still hindered with problems of rapid capacity fading and poor rate capability.

In an attempt to overcome these significant drawbacks, one typical approach has been developed: synthesizing nanostructured Fe_2O_3 materials with various morphologies, including nanoparticles [13], nanocubes [14], nanorods [15], nanowires [16] and nanotubes [17]. The nanostructures facilitate both the electron and Li^+ transport by reducing diffusion paths; improve the intercalation kinetics by providing a larger electrode/electrolyte contact area [3]. These reported nanostructured Fe_2O_3 materials definitely show significant improvement in electrochemical performance. However, these nanomaterials often display relatively low volumetric energy density and show difficulties in the electrode film coating process, and so fail to meet both the energy and power demand for practical applications. One effective way is to prepare nanostructured micro-scale materials.

In this work, we report a simple, template-free, hydrothermal method for the production of hierarchical Fe_2O_3 microspheres assembled by uniform nanoparticles, where lysine acted as

* Corresponding authors. Tel./fax: +86 21 51630320.
E-mail addresses: huangt@fudan.edu.cn (T. Huang), asyu@fudan.edu.cn (A. Yu).

0378-7753/$ – see front matter © 2012 Elsevier B.V. All rights reserved.
http://dx.doi.org/10.1016/j.jpowsour.2012.08.057

a hydrolysis-controlling agent. This method is very facile and effective for preparing the microsphere materials in high yield and with uniform diameter. On the basis of the crystal structures, morphology's evolution with time and the comparative experiment with L-arginine, the possible formation mechanism of the Fe_2O_3 microspheres is also presented and discussed. The electrochemical properties of the as-prepared Fe_2O_3 hierarchical microspheres as LIBs anode materials are also investigated.

2. Experimental

2.1. Preparation of Fe_2O_3 microspheres

The Fe_2O_3 microspheres were prepared through a simple hydrothermal reaction. All reagents are analytically pure and used without further purification. In a typical experiment, 2 g lysine and 1.3515 g $FeCl_3 \cdot 6H_2O$ were dissolved in 30 mL deionized water, the solution was homogenized by vigorous stirring. The result mixture was transferred to a 50 mL Teflon-lined autoclave and then maintained at 180 °C for 12 h. After reaction, the autoclave cooled to room temperature naturally. The products were obtained by centrifuging and sequentially washing with water and ethanol for several times and then dried in a vacuum oven at 60 °C for 12 h.

To investigate the growth mechanism of the Fe_2O_3 microspheres, several experiments that involved intercepting the intermediates at different hydrothermal reaction times were performed. The hydrothermal reaction was conducted for 4 h, 8 h and 12 h. For comparison, samples were synthesized by using 2 g L-arginine and 1.3515 g $FeCl_3 \cdot 6H_2O$ under hydrothermal treatment at 180 °C for 4 h, 8 h and 12 h too.

2.2. Characterization and electrochemical measurements

The crystalline structure and morphology were characterized by X-ray diffraction (XRD, Bruker D8 Advance, Cu Ka radiation, = 1.5406Å), field-emission scanning electron microscopy (FE-SEM, Hitachi S-4800) and transmission electron microscopy (TEM, JEM-2100F). The specific surface area and pore size distribution of the sample were derived using the multipoint Braunauer–Emmett–Teller (BET) method and the Barrett–Joyner–Halenda (BJH) model, respectively.

Electrochemical tests were performed using a CR2016-type coin cell. An assembled coin cell was composed of lithium as the counter electrode and the working electrode consisting of 50% active material, 30% super P carbon black and 20% polyvinylidene fluoride (PVDF) made on copper foil. Coin-type cells were assembled in an argon-filled glove box (Mikarouna, Superstar 1220/750/900) with 1 M $LiPF_6$ solution in ethylene carbonate/diethyl carbonate (EC:DEC = 1:1, v/v) as the electrolyte and Celgard 2300 as the separator. The total mass of the active electrode material is about 2–3 mg and the electrode surface area is 1.54 cm^2 (Φ14 mm). The cyclic voltammetry (CV) measurement was performed on an Electrochemical Workstation (CH Instrument 660A, CHI Company) at a scan rate of 0.2 mV s^{-1} in the range of 3.0–0.01 V vs. Li/Li^+. The galvanostatic charge–discharge tests were performed on a battery test system (Land CT2001A, Wuhan Jinnuo Electronic Co. Ltd.) at a constant current density of 100 mA g^{-1} in the potential range from 0.01 to 3.0 V.

3. Results and discussion

3.1. Morphology and structure of Fe_2O_3 microspheres

The structure and chemical composition of the as-prepared Fe_2O_3 sample were confirmed with XRD. Fig. 1 illustrates the XRD pattern of the Fe_2O_3 microspheres after hydrothermal reaction at 180 °C for 12 h. Twelve obvious diffraction peaks can be easily identified for the (012), (104), (110), (113), (024), (116), (018), (214), (300), (208), (1010) and (220) planes of the pure hexagonal phase α-Fe_2O_3 crystalline structure, respectively, which are consistent with the standard spectrum (JCPDS No. 33-0664). By using Scherrer's formula based on the peaks of (012), (104), (110), and (024) and (116), the grain size of Fe_2O_3 is estimated to be 47.04 nm.

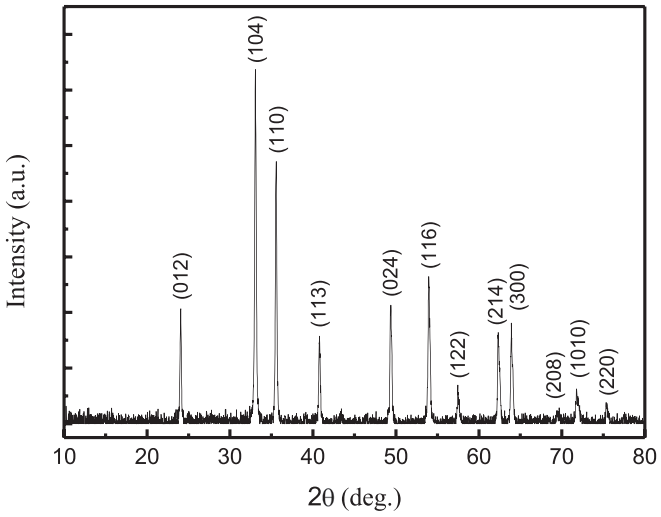

Fig. 1. XRD pattern of Fe_2O_3 microspheres after hydrothermal reaction at 180 °C for 12 h.

Fig. 2a shows the SEM image of the uniform Fe_2O_3 microspheres with a diameter of 2 μm, which is accumulated by evenly distributed nanoparticles of about 50 nm, as revealed by the magnified region of a single microsphere (Fig. 2b) in Fig. 2c. Mesopores formed among the nanoparticles produce a hierarchical porous structure in the crystalline Fe_2O_3 microspheres.

To further examine the architecture of the Fe_2O_3 microspheres, the samples were investigated by TEM technique. Fig. 3a shows a representative monodispersed Fe_2O_3 microsphere. Its diameter is about 1.75 μm, in good agreement with the SEM result (Fig. 2a). As shown in Fig. 3b, the Fe_2O_3 microsphere's structure is actually constructed from the assembly of interconnected nanoparticles. The crystallite size is match well with the SEM and XRD results mentioned above. Further evidence for the porous structure can also be found from Fig. 3b.

To gain further insight into the porous structure and pore size distribution of the Fe_2O_3 nano/micro superstructure, Brunauer–Emmett–Teller (BET) measurements were performed. As shown in Fig. 4a, the nitrogen adsorption–desorption isotherm can be attributed to type IV with a distinct hysteresis loop observed in the range of 0.5–1.0 P/P_0. The as-obtained Fe_2O_3 microspheres have a small BET surface area of 15 m^2 g^{-1}, which is primarily due to the formation of micro-scale spherical secondary particles. This helps improve its volumetric energy density dramatically as an anode material and favors electrode fabrication by easy control of the thickness of the electrode film in practical production. From the pore size distribution curve in Fig. 4b, nanopores between 3 and 10 nm indicate the nanoporous feature present in the as-obtained Fe_2O_3 microspheres, which results from the accumulation of nanosized particles.

3.2. Formation mechanism of Fe_2O_3 microspheres

It is well known that the pH of amino acids depends upon the amount of both the amino-group and the carboxylic acid group in their molecular structures, due to the existence of the hydrolysis

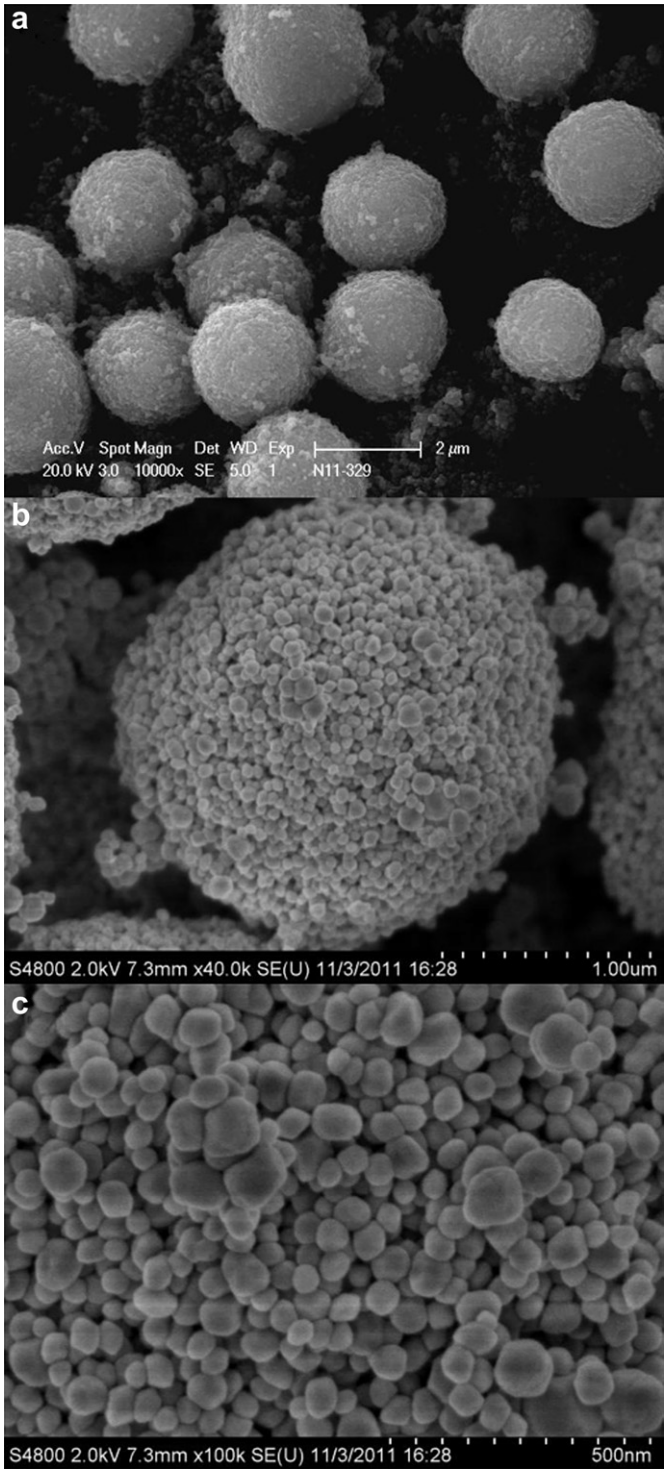

Fig. 2. Morphologies of Fe_2O_3 microspheres after hydrothermal reaction at 180 °C for 12 h: (a) low magnification SEM image; (b) high magnification SEM image; and (c) nanosized primary particles of one microsphere.

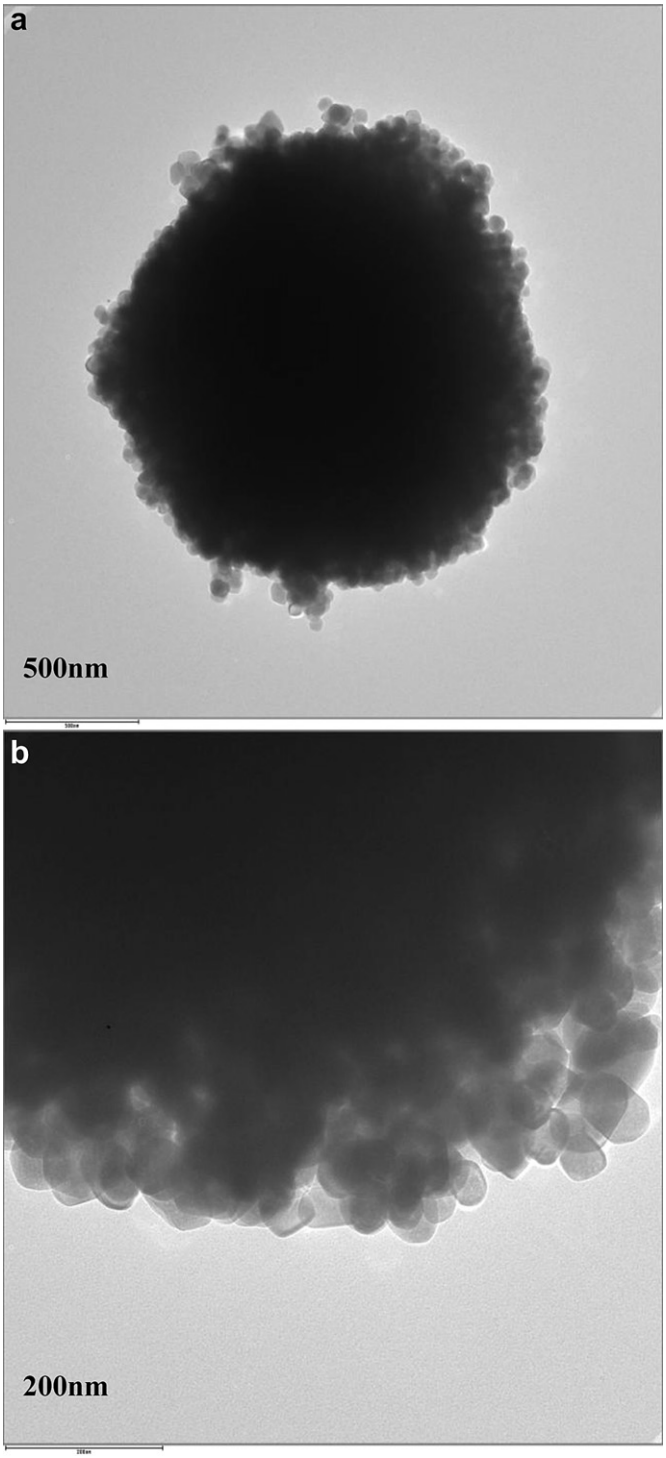

Fig. 3. TEM images of Fe_2O_3 microspheres after hydrothermal reaction at 180 °C for 12 h: (a) low magnification; and (b) high magnification.

process. Lysine is an amino acid with two amino groups and one carboxylic acid group, its pH should be commonly above 7, it means that the lysine can be applied as a hydrolysis-controlling agent for the formation of Fe_2O_3 under the hydrothermal treatment in this work. With the hydrolysis of lysine during the hydrothermal process, more and more OH^- come into being and the pH value of the solution increases greatly, which result in the formation of $Fe(OH)_3$ phase, and finally Fe_2O_3 form through dehydration of the hydroxides. The process can be shown as the following equations:

$$H_2N(CH_2)_3CH(NH_2)COOH + H_2O \leftrightarrow [H_3N(CH_2)_3CH(NH_2) \times COOH]^+ + OH^-$$

$$Fe^{3+} + 3OH^- \rightarrow Fe(OH)_3$$

$$2Fe(OH)_3 \rightarrow Fe_2O_3 + 3H_2O$$

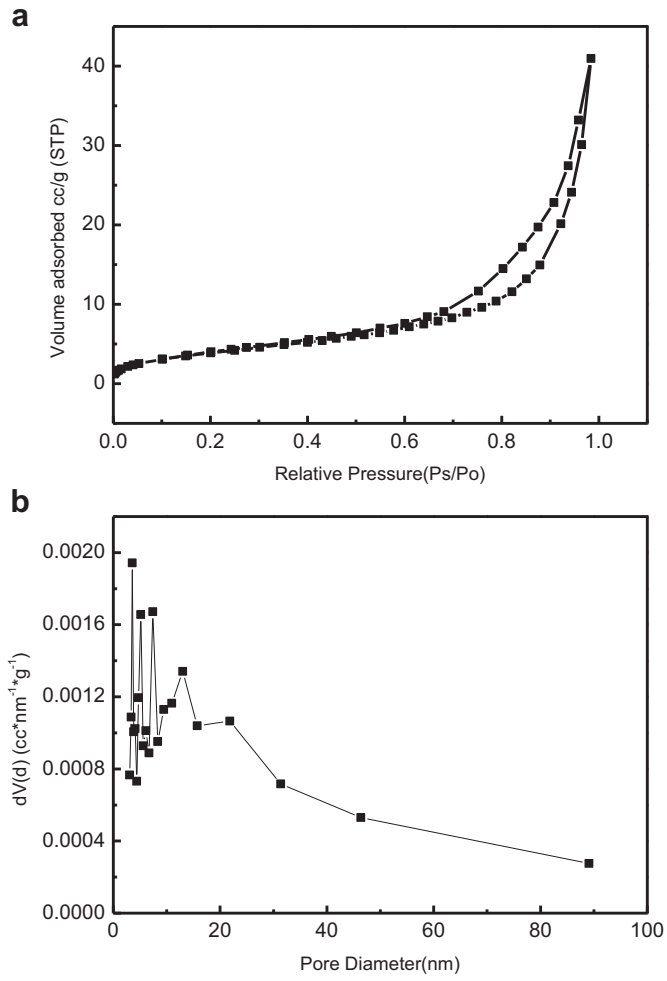

Fig. 4. The gas (N_2) adsorption–desorption isotherm loop (a) and BJH pore size distribution (b) of Fe_2O_3 microspheres after hydrothermal reaction at 180 °C for 12 h.

For the sake of clarifying the formation process of the unique Fe_2O_3 microspheres, the various Fe_2O_3 samples were synthesized by adjusting hydrothermal treatment time. Fig. 5 demonstrates the SEM images of the Fe_2O_3 samples obtained after different hydrothermal time. Obviously, after 4 h, Fe_2O_3 nanoparticles could be obtained (Fig. 5a), with the average size of 50 nm. While the Fe_2O_3 nanoparticles with quite high surface energy in the solution, these monodispersed nanoparticles tend to aggregate to decrease the surface energy by reducing the exposed areas [18,19]. Therefore, with the hydrothermal time of 8 h, as seen from Fig. 5b, the Fe_2O_3

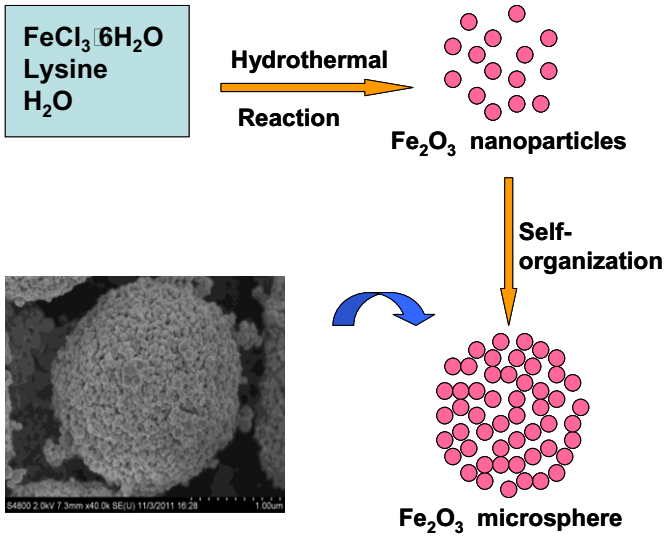

Fig. 6. Schematic for the formation mechanism of Fe_2O_3 microspheres.

microspheres occur, accompanying with some nanoparticles. With further hydrothermal treatment for 12 h, well-developed nanoparticles-based Fe_2O_3 hierarchical microspheres form through the self-assembly growth mechanism. Based on the investigation and analysis above, we propose the formation mechanism of the Fe_2O_3 microspheres as shown in Fig. 6.

However, according to the previous investigations, when choosing ammonia–water (w, 25%), distilled water or NaOH as a hydrolysis-controlling agent, Fe_2O_3 nanopolyhedra, nanoparticles and nanoflakes are obtained correspondingly [20,21]. Now, another question arises, expect for spontaneous energy-minimizing self-organization growth mechanism, does lysine play an important role in the formation of the unique hierarchical microspheres? To support this judgment, we choose 2 g L-arginine as a new hydrolysis-controlling agent to synthesize Fe_2O_3 samples, using 1.3515 g $FeCl_3 \cdot 6H_2O$ during the hydrothermal process. L-arginine is another unique amino acid with one guanido-group, one amino-group and one carboxylic acid, due to the existence of the hydrolysis process, its pH is commonly above 7 too. Fig. 7 shows the SEM images of the Fe_2O_3 samples synthesized by using L-arginine as the hydrolysis-controlling agent. After 4 h, a few of Fe_2O_3 nanoparticles could be obtained (Fig. 7a), with the average size of 100 nm. When the hydrothermal time prolonged to 8 h (Fig. 7b), the Fe_2O_3 nanoparticles with the same shape and size as these of reaction time of 4 h were gained, except that the amount increased. With further hydrothermal treatment for 12 h, the agglomeration of particles occurred (Fig. 7c). According to the results discussed

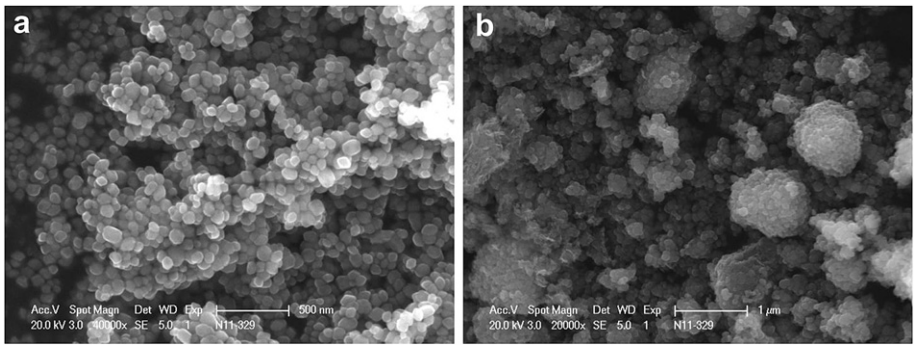

Fig. 5. SEM images of Fe_2O_3 synthesized after various hydrothermal times: (a) 4 h; and (b) 8 h.

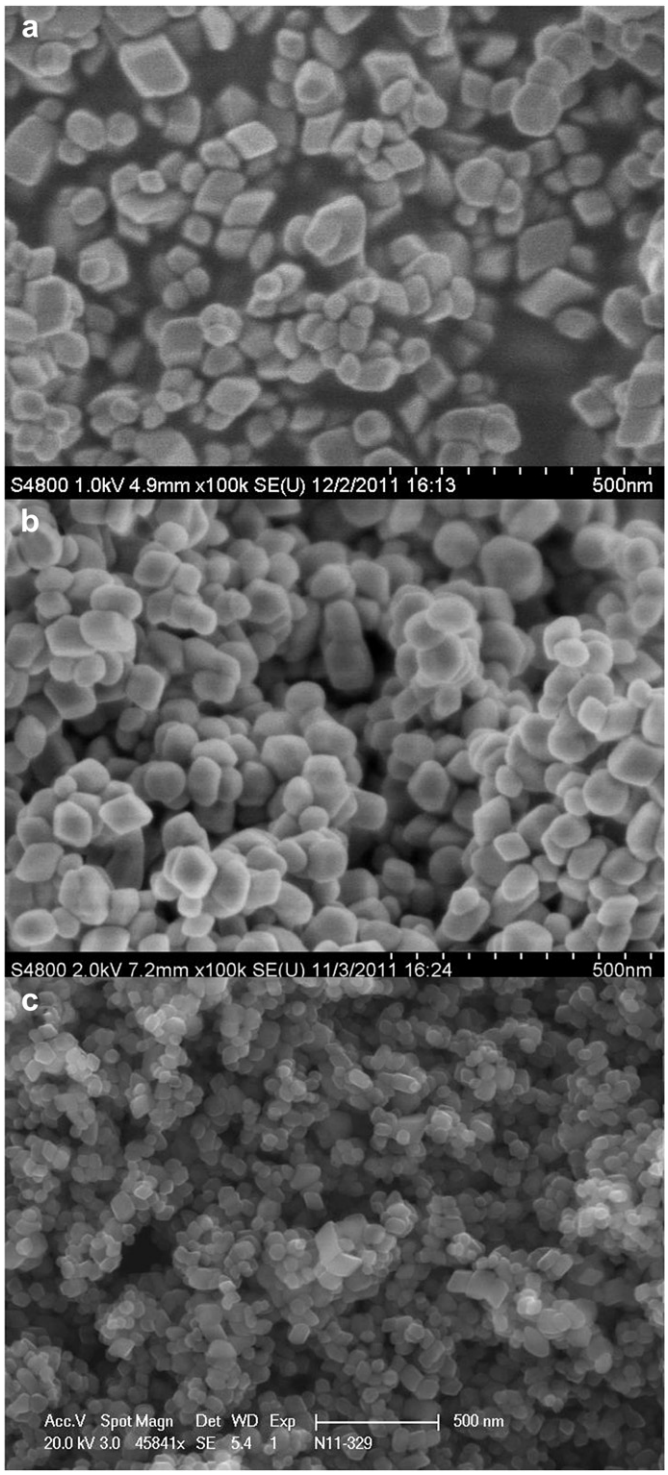

Fig. 7. SEM images of Fe_2O_3 synthesized by choosing L-arginine as the hydrolysis-controlling agent (2 g L-arginine and 1.3515 g $FeCl_3 \cdot 6H_2O$): (a) 4 h; (b) 8 h; and (c) 12 h.

above, we can conclude that for the case of using L-arginine as the hydrolysis-controlling agent, the reaction time of 8 h should be the best choice. So we then studied the electrochemical performance of Fe_2O_3 nanoparticles using L-arginine for 8 h. It also can be seen that when using L-arginine as the hydrolysis-controlling agent, no microsphere can be observed during the reaction. Obviously, it demonstrates that lysine is also an important factor to facilitate the formation of the Fe_2O_3 hierarchical microspheres.

3.3. Electrochemical performance

The electrochemical properties of the Fe_2O_3 microspheres using lysine as the hydrolysis-controlling agent, hydrothermal reacting at 180 °C for 12 h and the Fe_2O_3 nanoparticles using L-arginine as the hydrolysis-controlling agent, hydrothermal reacting at 180 °C for 8 h as anode materials for LIBs were investigated. The CV profiles of the Fe_2O_3 microspheres and the Fe_2O_3 nanoparticles for the initial two cycles are shown in Fig. 8a and b, respectively. As seen from Fig. 8a, two cathodic current peaks positioned at 1.64 and 0.68 V can be observed in the first cycle. The high intensity peak initially located at 0.68 V shifts to higher potential (0.79 V), and the other peak (1.64 V) disappears in the subsequent process. This can be explained by two factors: (1) the lithium insertion into the crystal structure of Fe_2O_3, the reversible conversion reaction of Fe_2O_3 with metallic lithium to form lithia (Li_2O) and metal (Fe^0), and (2) electrolyte decomposition to form SEI films [11,22]. Meanwhile, in the anodic process, a broad peak is present at about 1.65 V, corresponding to the reversible oxidation of Fe^0 to Fe^{3+} [23]. In the subsequent cycle, the anodic peak remains unchanged.

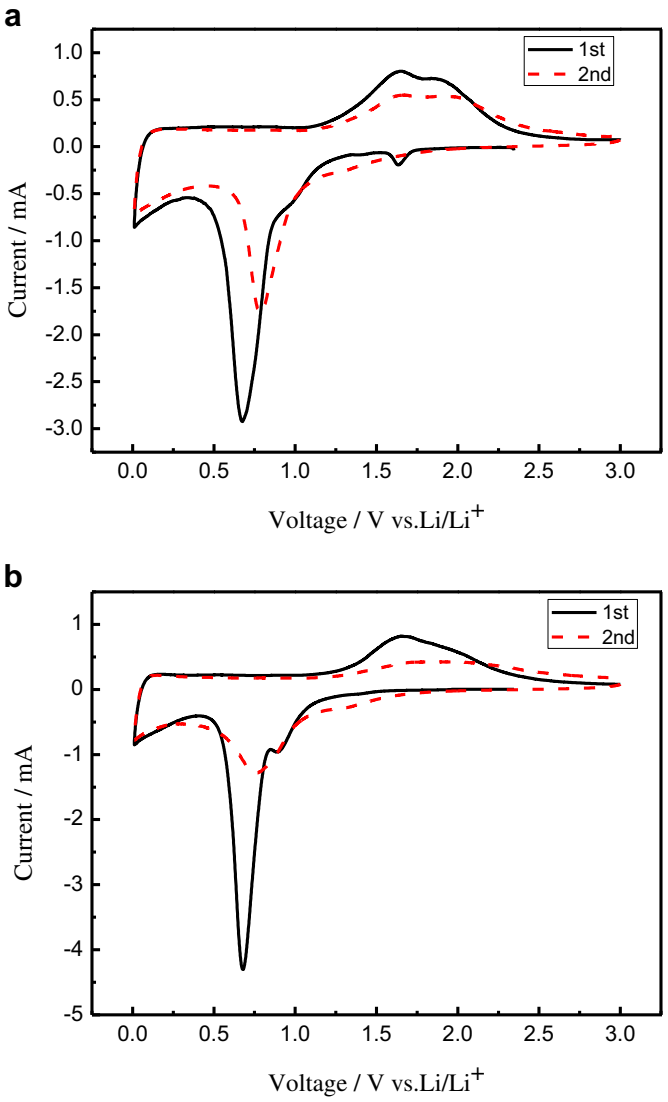

Fig. 8. Cyclic voltammograms of (a) Fe_2O_3 microspheres (lysine, hydrothermal reaction at 180 °C for 12 h); and (b) Fe_2O_3 nanoparticles (arginine, hydrothermal reaction at 180 °C for 8 h), from the first cycle to the second cycle at a scan rate of 0.2 mV s^{-1} in the voltage range of 0.01–3.0 V.

Additionally, peak intensities decrease, which can be attributed to the thermodynamically impossible extraction of Li from Li_2O and the decomposition of electrolyte to form a SEI layer [24]. Besides, caused by the polarization of the Fe_2O_3 in the first cycle, both cathodic and anodic peaks are positively shifted in the subsequent cycle. For the Fe_2O_3 nanoparticles shown in Fig. 8b, in the first cycle, there are two peaks at about 0.68 V and 0.9 V in the cathodic process, one broad peak at about 1.66 V in the anodic process. The condition of the second cycle is very similar with that of the Fe_2O_3 microspheres, which has been discussed above.

The charge/discharge curves of the as-prepared Fe_2O_3 microspheres and the Fe_2O_3 nanoparticles for the first three cycles obtained at a current density of 100 mA g^{-1} in the voltage window of 0.01–3.0 V (vs. Li/Li^+) are compared and presented in Fig. 9a and b, respectively. It can be seen that the first specific discharge capacity of the Fe_2O_3 microspheres is as high as 1477 mA h g^{-1}. From the fully discharged state, 73% (1079 mA h g^{-1}) of the stored lithium can be extracted upon charging to 3.0 V. For the Fe_2O_3 nanoparticles, they deliver the initial discharge and charge capacities of 1426 and 971 mA h g^{-1}, respectively, showing a Coulmobic efficiency of 68%. It is noted that the initial discharge capacity is even higher than the theoretical capacity of Fe_2O_3. This phenomenon has been widely reported for transition metal oxides [25,26], which is usually ascribed to the formation of the SEI film and possibly interfacial lithium storage.

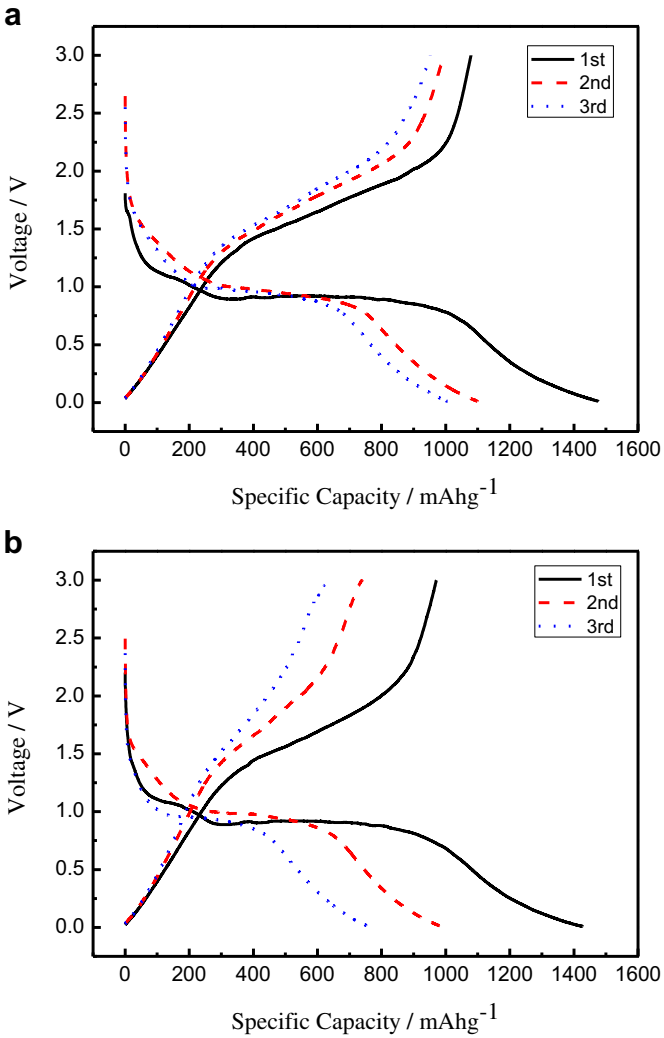

Fig. 9. The first three discharge/charge profiles of (a) Fe_2O_3 microspheres (lysine, hydrothermal reaction at 180 °C for 12 h); and (b) Fe_2O_3 nanoparticles (arginine, hydrothermal reaction at 180 °C for 8 h), at a current density of 100 mA g^{-1}, in the voltage range of 0.01–3.0 V.

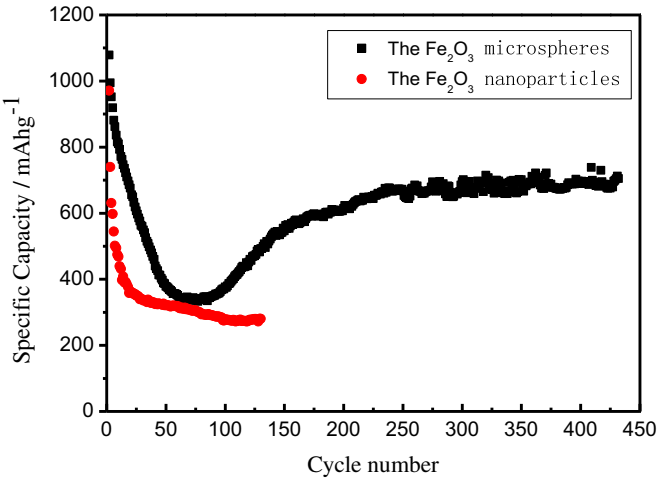

Fig. 10. Cycling performance of Fe_2O_3 microspheres (lysine, hydrothermal reaction at 180 °C for 12 h) and Fe_2O_3 nanoparticles (arginine, hydrothermal reaction at 180 °C for 8 h) at the current density of 100 mA g^{-1}.

Fig. 10 shows the cycling performance of the Fe_2O_3 microspheres and the Fe_2O_3 nanoparticles at a current density of 100 mA g^{-1}. It can be seen that the Fe_2O_3 microspheres exhibit a high reversible capacity of 705 mA h g^{-1} after 430 cycles. However, for the Fe_2O_3 nanoparticles, a much lower capacity of 281 mA h g^{-1} is delivered at the end of the 130 cycles and tends to be stable. Apparently, the Fe_2O_3 microspheres demonstrate a much better cyclic retention than the Fe_2O_3 nanoparticles. Interestingly, it is noted that the charge capacity of the Fe_2O_3 microspheres decreases first, then increases slightly and finally stabilizes. This phenomenon is likely due to the collapse of the microspheres during cycling. When it occurred, the inner particles which can not contact with the electrolyte before will exhibit their ability of lithium storage. To support this judgment, we investigate the electrode after being cycled. The SEM image of the electrode is shown in Fig. 11. It can be seen that the microspheres disappear after being cycled; instead, nanoparticles with size of 50–100 nm occur. It is an experimental evidence for the guess mentioned above. This change will increase the total surface area of the electrode material so that the contact

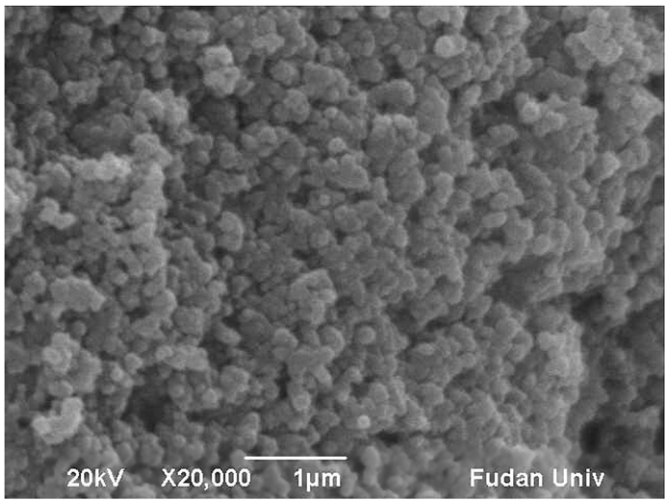

Fig. 11. SEM image of the electrode after being cycled.

area between the active material and electrolyte will largely increase. As a result, the capacity increases as observed in Fig. 10.

4. Conclusions

In summary, we have developed a facile lysine-assisted template-free approach to fabricate hierarchical porous Fe_2O_3 microspheres consisting of interconnected Fe_2O_3 nanoparticles. The formation of such unique Fe_2O_3 microspheres can be ascribed to the crystallization-assembly mechanism. Meanwhile, the comparative experiments confirmed that lysine plays a great role in the process. Electrochemical data show that a large initial charge specific capacity of 1079 mA h g^{-1} was obtained at a current density of 100 mA g^{-1}. Interestingly, the capacity of the product shows two different trends during cycling which are rarely reported in the literature, and remains 705 mA h g^{-1} after 430 cycles. In view of their excellent lithium storage properties and simplicity in synthesis, we believe that such a unique Fe_2O_3 microsphere superstructure has considerable potential as an anode material for LIBs.

Acknowledgments

The authors acknowledge funding supports from the National Natural Science Foundation (No. 21173054) and Science & Technology Commission of Shanghai Municipality (No. 08DZ2270500), China.

References

[1] M. Armand, J.M. Tarascon, Nature 451 (2008) 652–657.
[2] J.M. Tarascon, M. Armand, Nature 414 (2001) 359–367.
[3] A.S. Arico, P. Bruce, B. Scrosati, J.M. Tarascon, W.V. Schalkwijk, Nat. Mater. 4 (2005) 366–377.
[4] P.G. Bruce, B. Scrosati, J.M. Tarascon, Angew. Chem. Int. Ed. 47 (2008) 2930–2946.
[5] P. Poizot, S. Laruelle, S. Grugeon, L. Dupont, J.M. Tarascon, Nature 407 (2000) 496–499.
[6] J. Maier, Nat. Mater. 4 (2005) 805–815.
[7] D. Larcher, D. Bonnin, R. Cortes, I. Rivals, L. Personnaz, J.M. Tarascon, J. Electrochem. Soc. 150 (2003) A1643–A1650.
[8] F. Jiao, J.L. Bao, P.G. Bruce, Electrochem. Solid-State Lett. 10 (2007) A264–A266.
[9] M.V. Reddy, T. Yu, C.H. Sow, Z.X. Shen, C.T. Lim, G.V. Subba Rao, B.V.R. Chowdari, Adv. Funct. Mater. 17 (2007) 2792–2799.
[10] C.Z. Wu, P. Yin, X. Zhu, C.Z. OuYang, Y. Xie, J. Phys. Chem. B 110 (2006) 17806–17812.
[11] H. Liu, G. Wang, J. Park, J. Wang, H. Liu, C. Zhang, Electrochim. Acta 54 (2009) 1733–1736.
[12] Z.C. Wu, K. Yu, S.D. Zhang, Y. Xie, J. Phys. Chem. C 112 (2008) 11307–11313.
[13] W.T. Dong, C.S. Zhu, J. Mater. Chem. 12 (2002) 1676–1683.
[14] P.R. Patil, S.S. Joshi, Synth. React. Inorg. Met. Org. Chem. 37 (2007) 425–429.
[15] X. Wang, X.Y. Chen, L.S. Gao, H.G. Zheng, M.R. Ji, C.M. Tang, T. Shen, Z.D. Zhang, J. Mater. Chem. 14 (2004) 905–907.
[16] L.C. Hsu, Y.Y. Li, C.Y. Hsiao, Nanoscale Res. Lett. 3 (2008) 330–337.
[17] Z.Y. Sun, H.Q. Yuan, Z.M. Liu, B.X. Han, X.R. Zhang, Adv. Mater. 17 (2005) 2993–2997.
[18] C.H. Jiang, E. Hosono, M. Ichihara, I. Honma, H.S. Zhou, J. Electrochem. Soc. 155 (2008) A553–A556.
[19] R.L. Penn, J.F. Banfield, Science 281 (1998) 969–971.
[20] J.M. Ma, J.B. Lian, X.C. Duan, X.D. Liu, W.J. Zheng, J. Phys. Chem. C 114 (2010) 10671–10676.
[21] L. Chun, X.Z. Wu, X.M. Lou, Y.X. Zhang, Electrochim. Acta 55 (2010) 3089–3092.
[22] S. Laruelle, S. Grugeon, P. Poizot, M. Dolle, L. Dupont, J.M. Tarasconz, J. Electrochem. Soc. 149 (2002) A627–A634.
[23] Y. Han, Y.J. Wang, L. Li, Y.P. Wang, L.F. Jiao, H.T. Yuan, S.X. Liu, Electrochim. Acta 56 (2011) 3175–3181.
[24] J. Chen, L.N. Xu, W.Y. Li, X.L. Gou, Adv. Mater. 17 (2005) 582–586.
[25] S.L. Chou, J.Z. Wang, D. Wexler, K. Konstantinov, C. Zhong, H.K. Liu, S.X. Dou, J. Mater. Chem. 20 (2010) 2092–2098.
[26] S.L. Jin, H.G. Deng, D.H. Long, X.J. Liu, L. Zhan, X.Y. Liang, W.M. Qiao, L.C. Ling, J. Power Sources 196 (2011) 3887–3893.